Proposed pathway for kinesin-1 backstepping

Algirdas Toleikis, Nicholas J. Carter & Robert A. Cross*

Centre for Mechanochemical Cell Biology, Warwick Medical School, Coventry CV4 7AL, UK. *Correspondence to: r.a.cross@warwick.ac.uk

Abstract

Kinesin-1 molecular motors are walking machines that step along microtubules. Their stepping action is heavily biased towards MT plus ends, but backsteps also occur, at a rate that depends on the load and the ATP concentration. Like forward steps, backsteps are typically 8nm, but larger backwards events also occur. These larger backwards events are thought to be slips rather than steps, because they are too fast to be composed of multiple, conventionally-coupled 8nm steps. Here we propose that not just these larger events, but all kinesin-1 backsteps, are slips. We find (1) that kinesin waits before forward steps for less time than before backsteps and detachments, (2) that kinesin waits for the same amount of time before backsteps and detachments, (3) that shifting kinesin from one type of MT lattice to another shifts the ratio of backsteps and detachments, without affecting forward stepping. Our findings indicate that forward kinesin steps originate from an earlier state in the mechanism than backsteps. Accordingly, we propose a revised scheme in which load-dependent ATP binding to the trailing kinesin head opens a time window devoted to ATP hydrolysis and forward stepping, whilst Pi release closes this window, creating a K.ADP.K.ADP state that can slip back along the MT, re-engage, release ADP, and retry ATP-driven forward stepping.

Significance statement

Kinesin-1 molecular motors typically move using a walking action towards microtubule plus ends. But kinesins also take backsteps, especially at high load. Backsteps are currently thought to occur by directional reversal of forwards walking. Here, we propose that these backward events are not steps, but slips. We report evidence that backwards translocations originate from a different and later state in the kinesin mechanism than the state that generates forward steps. In our proposed new scheme, kinesin-1 motors that fail to step forward within a load-dependent time window convert to a state that can slip back, re-engage with the microtubule, and try again to step forward.

Introduction

Kinesin-1 is a ubiquitous, ATP-driven molecular motor that moves in 8nm steps (1) towards the plus ends of cellular microtubules (MTs). To function successfully as an intracellular transporter (2)(3), kinesin needs to move vesicles and other cargo that can be up to several microns in diameter against appreciable hindering loads created by the crowded, and dynamic, intracellular environment. Understanding how kinesin makes sustained progress under dynamic load is an important problem. There is firm evidence that between steps, kinesin waits for ATP with one motor domain (the holdfast head) bound to the MT and the other (the tethered head), poised to step but prevented from doing so until ATP binds (4)(5)(6)(7)(8)(9)(10). At low hindering loads, forward steps, towards MT plus ends, predominate, whilst at higher loads, forward stepping slows down and more backsteps occur. It is clear that both forward steps (11)(12)(13) and backsteps (14)(15) require ATP. At stall, forward steps and backsteps are equally likely (14)(15) – indeed this property defines the stall force. Current models, including our own, envisage that backsteps occur by a hand-over-hand mechanism that resembles that for forward stepping, but with load-dependent reversal of the directional bias (14)(15)(16)(17)(18)(19). Nonetheless, it remains possible that forwards and backwards kinesin steps occur by different mechanisms.

To test this point experimentally, we compared the average dwell times for kinesin forward steps, backsteps and detachments. The dwell times are the waiting times preceding each step, consisting of the time spent waiting for ATP to bind plus the time taken to process ATP and complete the coupled mechanical step. We also made counts of forward steps, backsteps (on average 8 nm, but up to 12 nm), larger backsteps (> 12 nm) and full detachments for kinesin

stepping on GDP taxol brain MTs under defined hindering loads between 2 and 9 pN applied with an optical trap. (Fig. 1*A, B*). In a full detachment, the motor releases completely from the MT, causing the bead-motor complex to relax back into the centre of the optical trap (Fig. 1*A*).

Dwell times for forward steps are shorter than for backsteps

Using taxol-stabilised pig brain GDP MTs, the general form of the dwell time versus load relationship is as previously reported (14)(15)(16)(18), with forward step dwell times exponentially dependent on load at forces up to and including the stall force (Fig. 1*C*). Crucially however, we find that at substall loads, forward steps have shorter average dwell times than either backsteps or detachments (Fig. 1*C*), whilst backsteps and detachments have similar or identical average dwell times (see next section). Previous work, including our own, has assigned backsteps and forward steps as alternative outcomes from the same state in the kinesin mechanism (14, 15). Correspondingly, current kinesin schemes postulate a minimum of two bound mechanical states (Fig. 1*D*, Scheme 1). In Scheme 1, ATP binds to state 1, the waiting state, and converts it to state 2, the stepping state, which then either steps forward, or backward, or detaches, depending on load. Because forward and backward steps originate from the same state, their dwell times are drawn from the same distribution and their dwell time versus load relationships therefore superpose. However we now find that average dwells times for forward steps are shorter than those for backsteps and detachments. To explain this we need an extra state, with ATP binding creating state 2, the try-forward state, and Pi release creating state 3, the backstepping and detaching state (Fig. 1*D*, Scheme 2). Scheme 2 is the minimum scheme required to produce different dwell time distributions for forward and backwards steps.

The difference between average forward and backstep dwell times for GDP taxol brain MTs is just a few milliseconds at 3 pN load, increasing approximately exponentially to several tens of milliseconds at 6 pN load (Fig. 1*C*). On other types of MT lattice, average forward and backstep dwell times are more obviously different. We measured kinesin-1 single molecule stepping mechanics on brain GDP taxol MTs, brain GDP MTs without taxol, brain GMPCPP epothilone MTs and *S. pombe* GMPCPP epothilone MTs (Fig. 2). Epothilone is a MT-binding drug that stabilizes both brain and yeast MTs, whereas taxol only stabilizes brain MTs. Previous work has shown that the nucleotide state of tubulin can influence MT sliding velocity in unloaded motility assays (20). Further, lattice expansion and other lattice effects

due to nucleotide state (21) drug binding (22) or kinesin binding (23)(24) can potentially influence kinesin binding and stepping. Under load, we find that changing lattice type indeed substantially affects kinesin stepping mechanics. Most obviously, stalls last much longer on yeast (*S. pombe*) MTs (Fig. 2*A*) compared to brain MTs, (Fig. 2*B*), indicating that detachments at high force are more probable for brain MTs.

Dwell times for backsteps and detachments are the same

In more detail, for all types of MT lattice that we tried, we find that mean forward step dwell times at substall forces are shorter than those for backsteps and detachments, whilst mean dwell times for ~ 8 nm backsteps, longer backsteps and detachments appear identical. Median forward step dwell times are also shorter than median backstep and detachment dwell times, and median backstep and detachment dwell times similar or identical, for all types of MT lattice that we tried (Fig. S1). These findings reflect that the dwell time distributions for 8 nm backsteps, longer backsteps and detachments superpose, implying that these different types of events all originate from the same progenitor state (16)(18). Since backstep and detachment dwell times are longer, on average, than forward step dwell times, this state must occur later in each cycle of the mechanism than the state that generates forward steps (Fig. 1*D*, Scheme 2).

Counts of backsteps and detachments vary reciprocally on different MT lattices

Making counts of forward steps, backsteps and detachments at each load gives further insight. The balance between ~8 nm backsteps, longer backsteps and detachments at any particular load shifts substantially depending on the type of MT lattice, whilst the fraction of forward steps is little affected (Fig. 3*A*-*D*). The ratio #forward steps / #backsteps decreases exponentially with load, as previously reported (14)(15). However, both the exponential factor and the stall force, the force at which the #forward steps / #backsteps ratio is unity, are different for the different MT lattices. For GDP taxol brain MTs, stall force is 7.3±0.2 pN as previously reported (14)(15), whereas for the other types of MT, stall force is 6.4±0.1 pN (Fig. 3*E,* p-value < 0.001 vs GDP taxol brain MTs). By contrast, the relationship #forward steps / (#backsteps + #detachments) versus load is almost invariant for the different types of MT (Fig. 3*F*), reflecting that by varying MT lattice type the relative incidence of ~8 nm backsteps, longer backsteps and detachments can be changed, without appreciably changing the count of forward steps (Fig. 3*A*-*D*; Fig. S2) or the total count of #backsteps + #detachments at any particular load. This is only possible in a 3-state scheme (Fig. 1*D*),

where backsteps and detachments are alternative outcomes from state 3 and this state succeeds state 2, the state from which forward steps originate. Because detachments occur from state 3 and state 3 is also the progenitor for backsteps, we hypothesized that state 3 is a weak binding state that can diffuse back along the MT, potentially along an electrostatic guide rail, and then convert to strong binding to complete a backstep. To probe the nature of state 3, we varied conditions further.

Added ADP promotes and lengthens backsteps

K.ADP is the weakest state of the kinesin cycle (25)(26). If state 3 is a K.ADP state, then adding extra ADP to the bathing solution should enrich state 3 via ADP binding. To test this possibility, we recorded kinesin stepping on brain GDP taxol MTs in the presence of added ADP (Fig. 4*B*). Increasing [ADP] without changing [ATP] increases the incidence of backsteps and detachments whilst reducing the incidence of forward steps (Fig. 4*D;* Fig. S3*B*). Added ADP not only produces more backsteps, throughout the force range we tested, but also adds a population of longer backsteps (Fig. S4*B*). As a result of these effects, stall force is substantially reduced, from 7.3±0.2 to 5.1±0.2 pN (Fig. 4*E*). These data indicate that adding ADP enriches state 3, from which detachments and backsteps arise (Fig. 1*D*), consistent with state 3 being a K.ADP-K.ADP state and with added ADP exerting its effects by enriching the K.ADP-K.ADP state. We see also that added ADP reduces the mean forward step dwell time (Fig. S4*A*) at high loads, consistent with the main element of dwell time under load being the waiting time before nucleotide binding and with added ADP competing directly with ATP for binding to the waiting state, thereby depleting the population of longer dwells.

Increased ionic strength promotes detachment

By increasing ionic strength, we expect to weaken our hypothesised weakly bound K.ADP-K.ADP state 3, because weak binding has a considerable electrostatic component (27). We find that indeed increased ionic strength increases the incidence of detachments, with much smaller effects on the incidence of ~8 nm backsteps and longer backsteps (Fig. 4*C*; Fig. S4), consistent with it weakening the K.ADP-K.ADP state and driving its detachment, without appreciably affecting forward stepping. As a result, stall force is only marginally reduced (Fig. 4*E*).

Subtilisin treatment of MTs lengthens backsteps and inhibits detachment

Cleaving the C-terminal E-hook peptides of tubulin (28) has only slight effects on kinesin velocity at low load, but reduces processivity (29). To further probe for our envisaged semi-detached state, we cleaved the E-hooks from GDP-taxol MTs using subtilisin, and again examined stepping mechanics under load. Subtilisin digestion has little or no effect on dwell times under load compared to undigested GDP taxol MTs (Fig. S5), or on the tendency to take forward steps relative to all other events (Fig. 4*D* and *E;* Fig. S3*D*). It does however increase the probability of a backstep being long (>12 nm) (Fig. S3*D* & *F*) and decrease the probability of detachment. These data again demonstrate that the balance between short backsteps, long backsteps and detachments can be shifted substantially by experiment, without affecting forward stepping, consistent with backsteps and detachments originating from a different and later state in the kinesin cycle than forward steps.

Backsteps and detachments originate from a later state than forward steps

Our key finding is that backstep and detachment dwells are drawn from the same dwell time distribution, whilst forward steps are drawn from a different dwell time distribution with a shorter average dwell time. Scheme 2 (Fig. 1*D,* Scheme 2) is the minimum scheme necessary to explain these findings. Scheme 2 is needed to explain how shifting kinesin between different MT types can shift the balance between backsteps and detachments, without affecting forward stepping. Scheme 1, in which forward steps and backsteps originate from the same state, is ruled out, because it predicts that forward and backsteps have the same average dwell times at any particular load – and we have shown that they do not. How might scheme 2 map to the kinetic mechanism of kinesin?

Proposed Model

In our proposed new minimal model for the kinesin-1 mechanochemical cycle (Fig. 5), ATP binding gates forward stepping by triggering diffusion-to-capture of the tethered head (4)(30)(31)(5) and by stabilising neck linker docking (32)(33)(34)(35). We propose that ATP binding opens a time window devoted exclusively to ATP hydrolysis and forward stepping. Within this time window, our scheme allows for forward stepping under load from either the ATP or the ADP.Pi states of the holdfast head (blue pathway). We include both these possible pathways for forward stepping because whilst recent evidence points to the K.ADP.Pi - K.ADP state as the origin of forward steps at zero load (10), the effects of load on the hydrolysis step are not yet clear. It is possible, for example, that the hydrolysis step

might be reversible under load, as it is for myosin (36)(37). In our model, the forward-step time window is closed by Pi release (38) and we propose that backsteps and detachments occur only after Pi release. We envisage that at high hindering loads, forward stepping increasingly fails to occur within its time window and that closure of this time window by Pi release switches the motor rapidly into a semi-detached K.ADP - K.ADP state (orange pathway) state 3. In our scheme, this K.ADP - K.ADP state then typically slips back along the lattice, pulled by the optical trap, re-engages, releases ADP from the newly re-engaged head and so returns to its ATP-waiting state, completing a de facto backstep. We term this pathway the rescued detachment pathway. Under backwards load, re-engagement of the K.ADP - K.ADP slip-state typically occurs to the closest available tubulin heterodimer, resulting in an 8 nm backwards event. Less routinely, backwards events of 16 or 24 nm can occur, or the motor can fully detach. For completeness, we include a presumptively off-pathway transition, in which MT-activated ADP release occurs with the motor standing in place (grey arrows). It is unclear at present to what extent this pathway (true futile cycling; ATP turnover without motion) is populated. It is also unclear whether our K.ADP - K.ADP slip state unbinds and rebinds to the same protofilament (PF), or whether it can migrate to a different PF. We also do not know whether following a slip, the same head that detached then re-engages, or whether the two heads can swap over. Answering these questions will require further work.

Relationship to other models

Most published models assign the K.ADP state of kinesin as the weakest binding state in the cycle (25)(26). Our assignment of the K.ADP - K.ADP state as the progenitor for backward slips and detachments is consistent with this and with earlier models (10)(15)(39). The idea that some backwards events are slips is also not novel; 16 nm, 24 nm and larger backwards displacements have previously been assigned as slips, on the basis that they are too fast to represent a sequence of 8 nm steps that are each coupled to a full cycle of ATP turnover (15). The novel aspects of our scheme (Fig. 5) are (1) that the interlude between ATP binding and Pi release (the hydrolysis time) is devoted *exclusively* to forward stepping, (2) that all backwards events at substall loads are backslips (rescued detachments) and (3) that backslips and detachments arise from the same K.ADP - K.ADP progenitor state.

Our proposed scheme is consistent with recent work showing that the rate of kinesin stepping can be influenced either by supplying extra ADP to inhibit tethered head attachment or by

lowering ionic strength to strengthen the binding of the K.ADP state to the MT (10). At zero external load, backsteps are rarely seen, but our data suggest that similar effects may operate – that is, that increased [ADP] and ionic strength respectively enrich or deplete a weak-bound K.ADP - K.ADP slip-state (40). Our proposed scheme is also consistent with recent work showing that adding Pi extends the single molecule run length of kinesin-1 (38) under forwards load, because it predicts that adding Pi will enrich the K.ADP.Pi - K.ADP state and thereby delay the formation of the backslipping K.ADP - K.ADP state. Equally, our scheme is consistent with models in which slower ATP hydrolysis promotes forward stepping by promoting diffusion-to-capture by the tethered head (10)(41), because slower ATP hydrolysis would also extend the time-window for forward stepping.

We attempted to test this point directly using ATPγS, an ATP analogue that drives MT sliding assays at ~2-3% of ATP velocity (42). Using iSCAT at zero load, ATPγS was recently shown to support slow, erratic stepping of single kinesin-1 molecules (43). Under load in the optical trap, we find that ATPγS also drives slow and erratic stepping of kinesin (Fig. S6). However, we also find that the MT-activated rate of ATPγS turnover by kinesin in solution is only 6-7 fold lower than that for ATP. These data suggest that ATPγS is hydrolysed relatively rapidly, but has poor mechanochemical coupling, so that at present it does not provide a useful test of our scheme.

Implications

Most immediately, our proposed new model has implications for the mechanochemical coupling of kinesin. As with previous models, in our new model (Fig. 5) kinesin consumes more ATP at high loads, because backwards events consume ATP. In our scheme, even a single 8 nm backwards event will consume one ATP to slip back 8 nm and another to step forward again to its original position. Higher loads favour longer backslips (Fig. 3) and will require correspondingly more ATP-driven forward steps to regain the ground lost. In one sense, these ATP-driven backslips are futile, because they generate negative progress. In another sense however, they are far from futile, because they create the opportunity to retry forward stepping under load without letting go of the MT and losing all the ground previously gained. A further possible pathway for futile cycling is denoted by the grey arrow in Fig. 5, showing the possibility of MT-activated ADP release without stepping. At present we have no information on the flux through this pathway, which would also consume ATP, but without losing ground.

Whilst our data argue that the large majority of kinesin-1 backward translocations are slip and rebind events, it remains formally possible that a small fraction of true mechanical backsteps, as opposed to slips, is present. If so, these would originate from the same progenitor state as forward steps (Fig.1*D*, scheme 1) and draw from the same dwell time distribution as forward steps. This would tend to make the dwell time distribution for short (8nm) backsteps more like that for forward steps. Whereas we see no detectable difference between the dwell time distributions of short backsteps, long backsteps & detachments. On this basis we conclude that at least the great majority of backwards kinesin-1 translocations are slip and rebind events.

By rescuing motors that have failed to step forward and allowing them to rebind and try again to step forward, our proposed rescued detachment pathway increases the ultimate success rate for processive forward stepping, with a corresponding increase in stall force and the ability to do useful work at high load. These gains come at the expense of extra ATP consumption at high loads, with the net effect that the ATP cost of each net forward step increases substantially with load. Our proposed scheme thus allows kinesin to adjust its coupling ratio at high loads. By combining tight-coupled forward steps with loose-coupled backward slips, kinesin maximises processive forwards progress at high loads, at the expense of efficiency.

Materials and Methods

Kinesin-beads. Unmodified 560 nm diameter polystyrene beads (Polysciences) were mixed with purified recombinant full-length *Drosophila* kinesin-1 (12), serially diluted until only 1/3 of beads were motile. Experiments were performed in BRB80 buffer (80 mM K-PIPES (pH 7.0), 2 mM $MgSO_4$, 1 mM EGTA, 3 g/L glucose) with 1 mM ATP and glucose-catalase oxygen scavenging system and 10 µM taxol or 10 µM epothilone or with no drug.

Microtubules. Purified tubulin (either from porcine brain or from *S. pombe (α1, α2, β* isoforms (44)) was polymerized in BRB80 at 37°C for 45-60 min in the presence of 1 mM GTP and 2 mM $MgCl_2$. MTs were spun down and resuspended in BRB80 supplemented with taxol (Sigma-Aldrich) or epothilone (VWR International) to 20 µM. Since taxol is not effective on *S. pombe* MTs, epothilone was used instead in combination with GMPCPP. In the case of unstabilised GDP MTs, no drug was added but MTs were capped immediately following assembly using tubulin premixed with 1 mM GMPCPP and incubated for 1 h,

added to a final concentration of 1 μM. The capped MTs were spun down and resuspended in BRB80.

Flow cells. The flow cell surface was passivated with 0.1 mg/ml PLL-PEG and then with 0.1 mg/ml casein (Susos AG, Dübendorf, Switzerland). MTs were covalently attached to the coverslip surface using mild glutaraldehyde crosslinking to the APTES silanized surface (45).

Optical trapping. A custom-built optical trap (15) was used, equipped with a 6 W Nd:YAG 1064 nm laser (I E Optomech Ltd, Newnham, England). High ionic strength experiments were performed in BRB160, which is identical to BRB80 but with 160 mM K-PIPES. MTs were initially visualized by differential interference contrast (DIC) microscopy and beads moved into position above the MTs by steering the trap. Imaging was then switched to amplitude contrast and the image projected on to the quadrant photodiode detector. Data were recorded at 20 kHz and moving-average filtered to 1 kHz during analysis.

Data analysis. Data were analysed in R using custom-written code (available on request). Automated step-detection was implemented using t-test analysis. In the t-test analysis, 8 data points before the suspected step and 8 after the step were compared by t-test. The threshold t-value was set to 30 and the minimum step size to 5 nm. Dwell times were defined as the waiting time between two consecutive steps. ~30-40% of the longest dwells in each force bin were manually verified to ensure there were no undetected steps within these dwells. Only steps above 2 pN could reliably be detected and only these were processed. Below 3 pN backsteps were rare and above 8 pN forward steps were rare. For forward step:backstep ratio measurements, the force range 3-8 pN was analysed to ensure a sufficient number of both forward steps and backsteps. Each force bin includes data at the force shown ± 0.5 pN.

Acknowledgements

We thank Douglas Martin, Masanori Mishima, Douglas Drummond and Huong Thuy Vu for helpful feedback on the draft ms. **Funding:** This work was funded by a Wellcome Senior Investigator award to RAC, grant number 103895/Z/14/Z. **Author contributions:** AT performed all the experiments and analysed all the data. NC designed and built the optical trap. AT, NC and RC collaborated to design and interpret experiments and write the ms.

Competing interests: Authors declare no competing interests. **Data and materials availability:** All data will be made available.

References

1. S. M. Block, L. S. Goldstein, B. J. Schnapp, Bead movement by single kinesin molecules studied with optical tweezers. *Nature* **348**, 348–352 (1990).

2. E. Karsenti, Self-organization in cell biology: a brief history. *Nature reviews Molecular cell biology* **9**, 255–262 (2008).

3. N. Hirokawa, Y. Tanaka, Kinesin superfamily proteins (KIFs): Various functions and their relevance for important phenomena in life and diseases. *Experimental Cell Research* **334**, 16–25 (2015).

4. D. D. Hackney, Evidence for alternating head catalysis by kinesin during microtubule-stimulated ATP hydrolysis. *Proceedings of the National Academy of Sciences of the United States of America* **91**, 6865–6869 (1994).

5. M. C. Alonso, *et al.*, An ATP Gate Controls Tubulin Binding by the Tethered Head of Kinesin-1. *Science* **316**, 120–123 (2007).

6. T. Mori, R. D. Vale, M. Tomishige, How kinesin waits between steps. *Nature* **450**, 750–754 (2007).

7. N. R. Guydosh, S. M. Block, Direct observation of the binding state of the kinesin head to the microtubule. *Nature* **461**, 125–128 (2009).

8. J. O. L. L. Andreasson, *et al.*, Examining kinesin processivity within a general gating framework. *eLife* **4**, 1166 (2015).

9. H. Isojima, R. Iino, Y. Niitani, H. Noji, M. Tomishige, The Stepping Motion of Kinesin-1. *Nature Chemical Biology* **12**, 290–297 (2016).

10. K. J. Mickolajczyk, W. O. Hancock, Kinesin Processivity Is Determined by a Kinetic Race from a Vulnerable One-Head-Bound State. *Biophysical Journal* **112**, 2615–2623 (2017).

11. W. Hua, E. C. Young, M. L. Fleming, J. Gelles, Coupling of kinesin steps to ATP hydrolysis. *Nature* **388**, 390–393 (1997).

12. D. L. Coy, M. Wagenbach, J. Howard, Kinesin takes one 8-nm step for each ATP that it hydrolyzes. *Journal of Biological Chemistry* (1999) https:/doi.org/10.1074/jbc.274.6.3667.

13. M. J. Schnitzer, S. M. Block, Kinesin hydrolyses one ATP per 8-nm step. *Nature* **388**, 386–390 (1997).

14. M. Nishiyama, H. Higuchi, T. Yanagida, Chemomechanical coupling of the forward and backward steps of single kinesin molecules. *Nature Cell Biology* **4**, 790–797 (2002).

15. N. J. Carter, R. A. Cross, Mechanics of the kinesin step. *Nature* **435**, 308–312 (2005).

16. Y. Taniguchi, M. Nishiyama, Y. Ishii, T. Yanagida, Entropy rectifies the Brownian steps of kinesin. *Nat Chem Biol* **1**, 342–347 (2005).

17. N. R. Guydosh, S. M. Block, Backsteps induced by nucleotide analogs suggest the front head of kinesin is gated by strain. *Proceedings of the National Academy of Sciences* **103**, 8054–8059 (2006).

18. Y. Taniguchi, P. Karagiannis, M. Nishiyama, Y. Ishii, T. Yanagida, Single molecule thermodynamics in biological motors. *Biosystems* **88**, 283–292 (2007).

19. N. J. Carter, R. A. Cross, Kinesin backsteps. *Biochemical Society transactions* **40**, 400–403 (2012).

20. R. D. Vale, C. M. Coppin, F. Malik, F. J. Kull, R. A. Milligan, Tubulin GTP hydrolysis influences the structure, mechanical properties, and kinesin-driven transport of microtubules. *J. Biol. Chem.* **269**, 23769–23775 (1994).

21. A. A. Hyman, D. Chrétien, I. Arnal, R. H. Wade, Structural changes accompanying GTP hydrolysis in microtubules: information from a slowly hydrolyzable analogue guanylyl-(alpha,beta)-methylene-diphosphonate. *The Journal of Cell Biology* **128**, 117–125 (1995).

22. I. Arnal, R. H. Wade, How does taxol stabilize microtubules? *Current Biology* **5**, 900–908 (1995).

23. D. R. Peet, N. J. Burroughs, R. A. Cross, Kinesin expands and stabilizes the GDP-microtubule lattice. *Nature Nanotech* **13**, 386–391 (2018).

24. T. Shima, *et al.*, Kinesin-binding–triggered conformation switching of microtubules contributes to polarized transport. *J. Cell Biol.* **217**, 4164–4183 (2018).

25. L. Romberg, R. D. Vale, Chemomechanical cycle of kinesin differs from that of myosin. *Nature* **361**, 168–170 (1993).

26. I. M.-T. Crevel, A. Lockhart, R. A. Cross, Weak and Strong States of Kinesin and ncd. *Journal of molecular biology* **257**, 66–76 (1996).

27. S. Uemura, *et al.*, Kinesin-microtubule binding depends on both nucleotide state and loading direction. *Proceedings of the National Academy of Sciences* **99**, 5977–5981 (2002).

28. Y. Okada, N. Hirokawa, Mechanism of the single-headed processivity: Diffusional anchoring between the K-loop of kinesin and the C terminus of tubulin. *Proceedings of the National Academy of Sciences* **97**, 640–645 (2000).

29. S. Lakämper, E. Meyhöfer, The E-Hook of Tubulin Interacts with Kinesin's Head to Increase Processivity and Speed. *Biophysical Journal* **89**, 3223–3234 (2005).

30. D. D. Hackney, Pathway of ADP-Stimulated ADP Release and Dissociation of Tethered Kinesin from Microtubules. Implications for the Extent of Processivity †. **41**, 4437–4446 (2002).

31. R. A. Cross, *et al.*, The conformational cycle of kinesin. *Philosophical transactions of the Royal Society of London Series B, Biological sciences* **355**, 459–464 (2000).

32. S. Rice, *et al.*, A structural change in the kinesin motor protein that drives motility. *Nature* **402**, 778–784 (1999).

33. A. S. Khalil, *et al.*, Kinesin's cover-neck bundle folds forward to generate force. *Proceedings of the National Academy of Sciences* **105**, 19247–19252 (2008).

34. W. Hwang, M. J. Lang, M. Karplus, Free Energy Changes During Kinesin's Force-Generating Substep. *Biophysical Journal* **98**, 369a–1 (2010).

35. B. G. Budaitis, *et al.*, Neck linker docking is critical for Kinesin-1 force generation in cells but at a cost to motor speed and processivity. *eLife* **8**, e44146 (2019).

36. C. R. Bagshaw, M. Adppp, Oxygen exchange in the y-phosphoryl group of protein-bound ATP during Mg2+-dependent adenosine triphosphatase activity of myosin. 5.

37. M. R. Webb, D. Trentham, The Mechanismof ATP Hydrolysis Catalyzed by Myosin and Actomyosin, usingRapid Reaction Techniquesto Study Oxygen Exchange. 7.

38. B. Milic, J. O. L. Andreasson, W. O. Hancock, S. M. Block, Kinesin processivity is gated by phosphate release. *Proceedings of the National Academy of Sciences of the United States of America* **111**, 14136–14140 (2014).

39. K. Sasaki, M. Kaya, H. Higuchi, A Unified Walking Model for Dimeric Motor Proteins. *Biophysical Journal* (2018).

40. R. Cross, The kinetic mechanism of kinesin. *Trends in Biochemical Sciences* **29**, 301–309 (2004).

41. W. O. Hancock, The Kinesin-1 Chemomechanical Cycle: Stepping Toward a Consensus. *Biophysical Journal* **110**, 1216–1225 (2016).

42. T. Shimizu, Nucleotide specificity of the enzymatic and motile activities of dynein, kinesin, and heavy meromyosin. *The Journal of Cell Biology* **112**, 1189–1197 (1991).

43. K. J. Mickolajczyk, *et al.*, Kinetics of nucleotide-dependent structural transitions in the kinesin-1 hydrolysis cycle. *Proceedings of the National Academy of Sciences* **112**, E7186–E7193 (2015).

44. D. R. Drummond, *et al.*, Purification of tubulin from the fission yeast Schizosaccharomyces pombe. *Methods in molecular biology (Clifton, N.J.)* **777**, 29–55 (2011).

45. M. P. Nicholas, L. Rao, A. Gennerich, Covalent immobilization of microtubules on glass surfaces for molecular motor force measurements and other single-molecule assays. *Methods in Molecular Biology* (2014) https:/doi.org/10.1007/978-1-4939-0329-0_9.

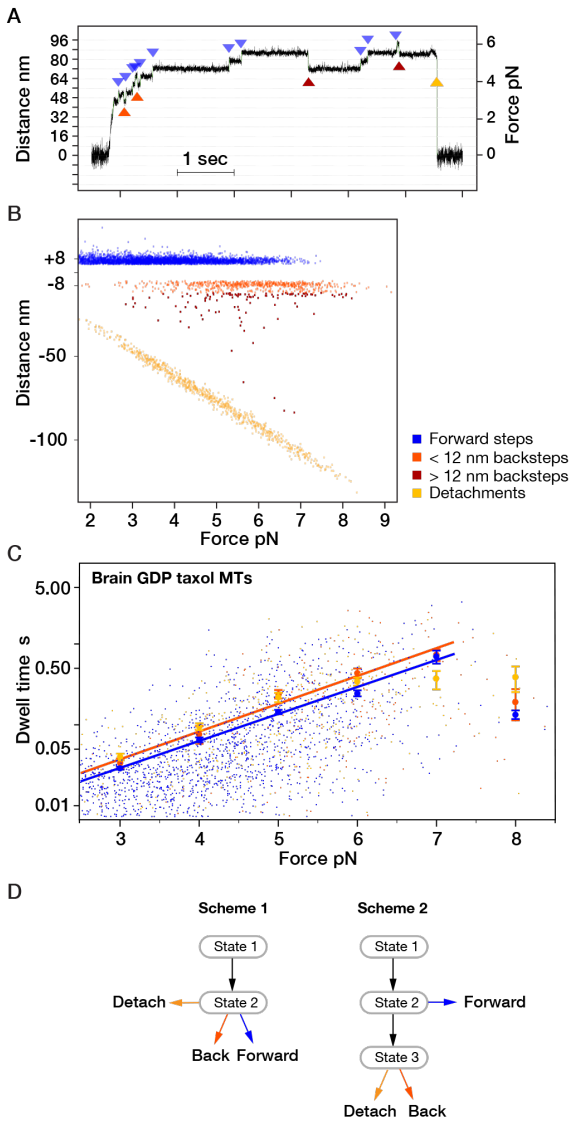

Fig. 1. Stepping of single kinesin molecules on brain GDP taxol MTs under load. (*A*) representative sequence of kinesin steps, with examples of each step-class highlighted. (*B*) Step amplitudes and incidence versus hindering force for forward steps, backsteps, larger backsteps and detachments. Trap stiffness for these experiments was ~0.06 pN/nm. (*C*) Forward step (blue), backstep (red) and detachment (yellow) dwell times vs. hindering force for Brain GDP MTs stabilised with taxol. The larger symbols are mean dwell times calculated for bins set at 1 pN intervals. Below stall, dwell times depend exponentially on load, forward step dwell times are characteristically shorter than backstep or detachment dwell times and backstep and detachment dwell times are indistinguishable. Approaching stall force on all types of MT, dwell times reach a plateau, above which further increases in force have little influence on dwell time (15). Mean dwells up to the stall force (7.2 pN) were fit by least squares using log(y) = kx + b. Parameters: blue: k=0.77, b=-5.7 orange: k=0.79, b=-5.6; Errors are SEM. (*D*) Minimal schemes for the kinesin mechanism (see text).

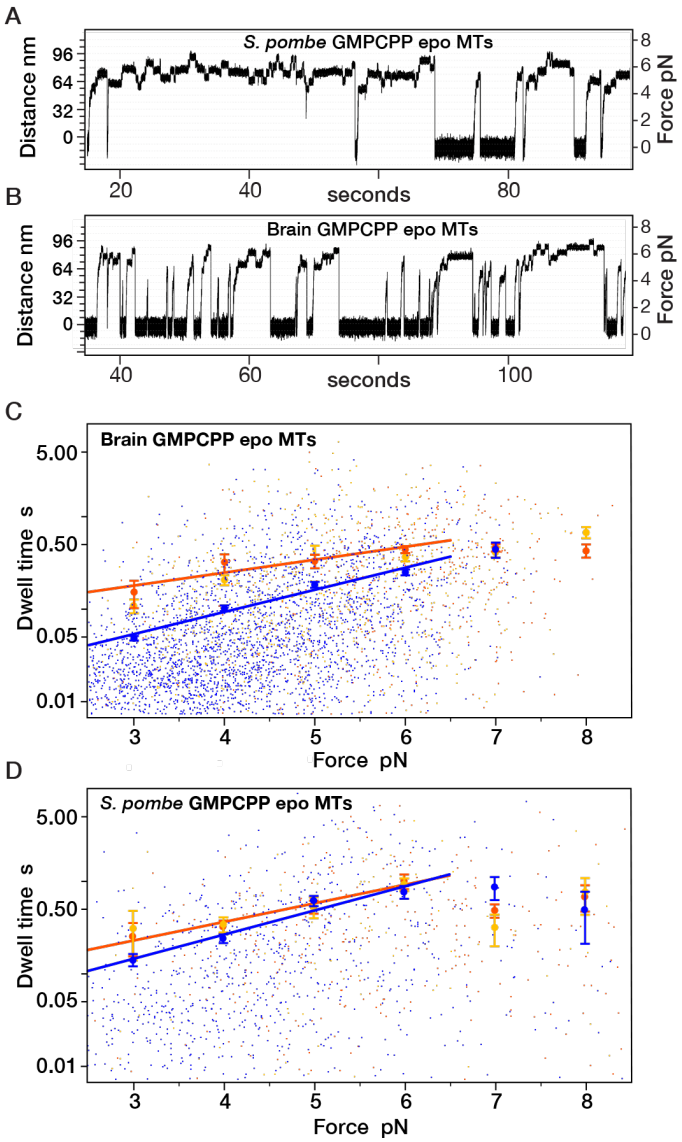

Fig. 2. Mechanics of kinesin stepping under load on different MT types. (*A,B*) optical trapping position versus time traces showing the much longer stalls typically seen with *S. pombe* GMPCPP epothilone MTs (*A*) compared to brain GMPCPP epothilone MTs (*B*). (*C,D*) Dwell times versus load for kinesin stepping on (*C*) Brain GMPCPP epothilone MTs and (*D*) *S. pombe* GMPCPP epothilone MTs. As in Fig 1C, dwell times depend exponentially on load, mean forward step dwell times are characteristically shorter than mean backstep or detachment dwell times and mean backstep and detachment dwell times are indistinguishable. Approaching stall force, backstep dwell times reach a plateau, above which further increases in hindering load have little effect on dwell time (15). Mean dwell times in the region below stall force were fit using log(y) = kx + b. Parameters: (C) blue: k=0.53, b=-4.4; orange: k=0.25, b=-2.3; (D) blue: k=0.6, b=-3.6; orange: k=0.46, b=-2.7; Errors are SEM.

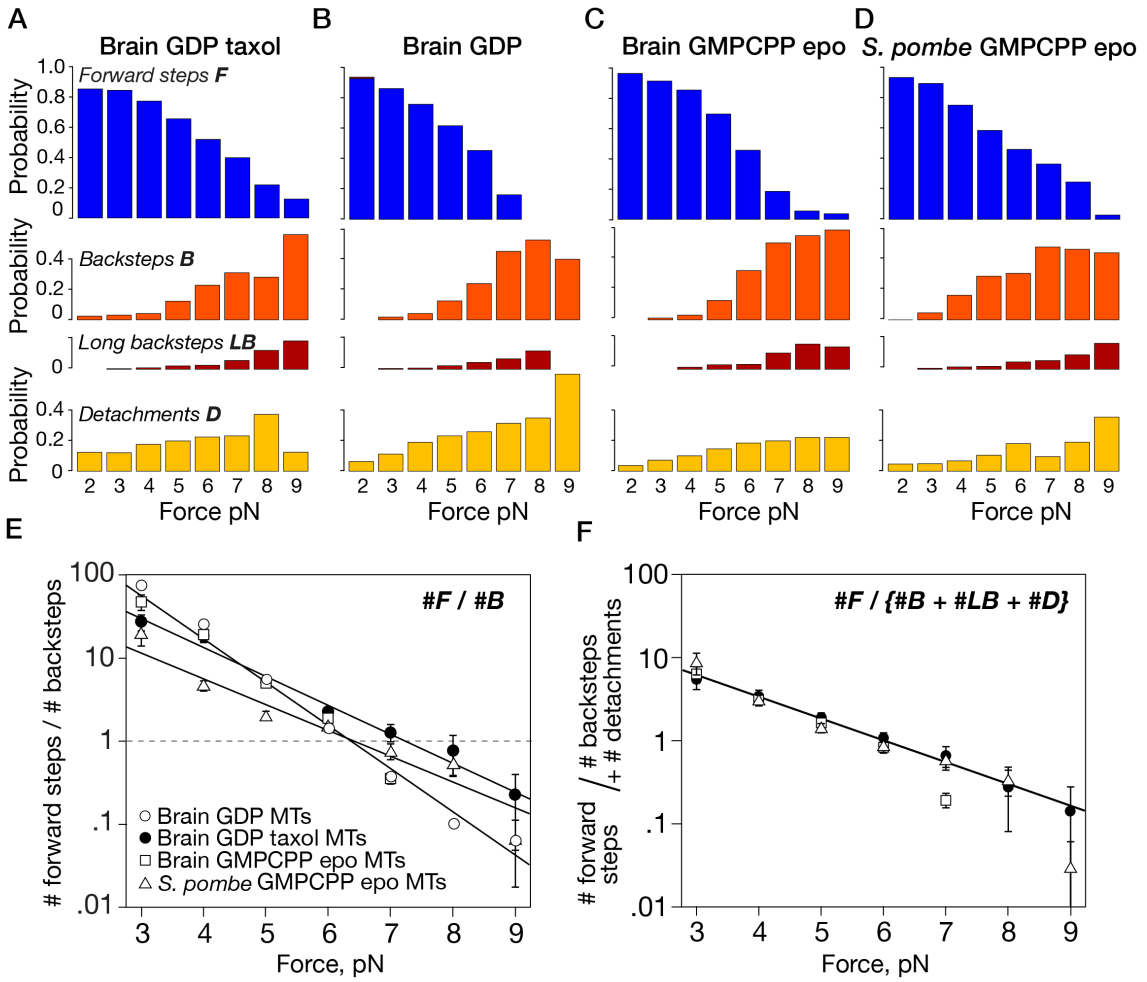

Fig. 3. Effects of changing MT type of step-event probabilities under load.

(*A-D*) Probability of forward steps (blue), <12 nm backsteps (orange), >12 nm backsteps (magenta) and detachments (yellow) versus force for kinesin stepping on (A) Brain GDP taxol MTs, (B) Brain GDP MTs (C) Brain GMPCPP epothilone MTs (D) *S. pombe* GMPCPP epothilone MTs. (*E*) #forward steps / #backsteps vs. force, for kinesin stepping on these four different MT types. Data were fit to log(y) = kx + b, weighting the fit by the reciprocal SE. For brain GMPCPP epothilone MTs k=-1.16, b=7.45; for *S. pombe* GMPCPP epothilone MTs k=-0.79, b=5.0, for brain GDP taxol MTs: k=-0.83, b=5.9. Errors are SE. (*F*) #forward steps / {#backsteps + #larger backsteps + #detachments}versus force, for kinesin stepping on different MT types. Fit shown is to taxol data: k=-0.58, b=3.5.

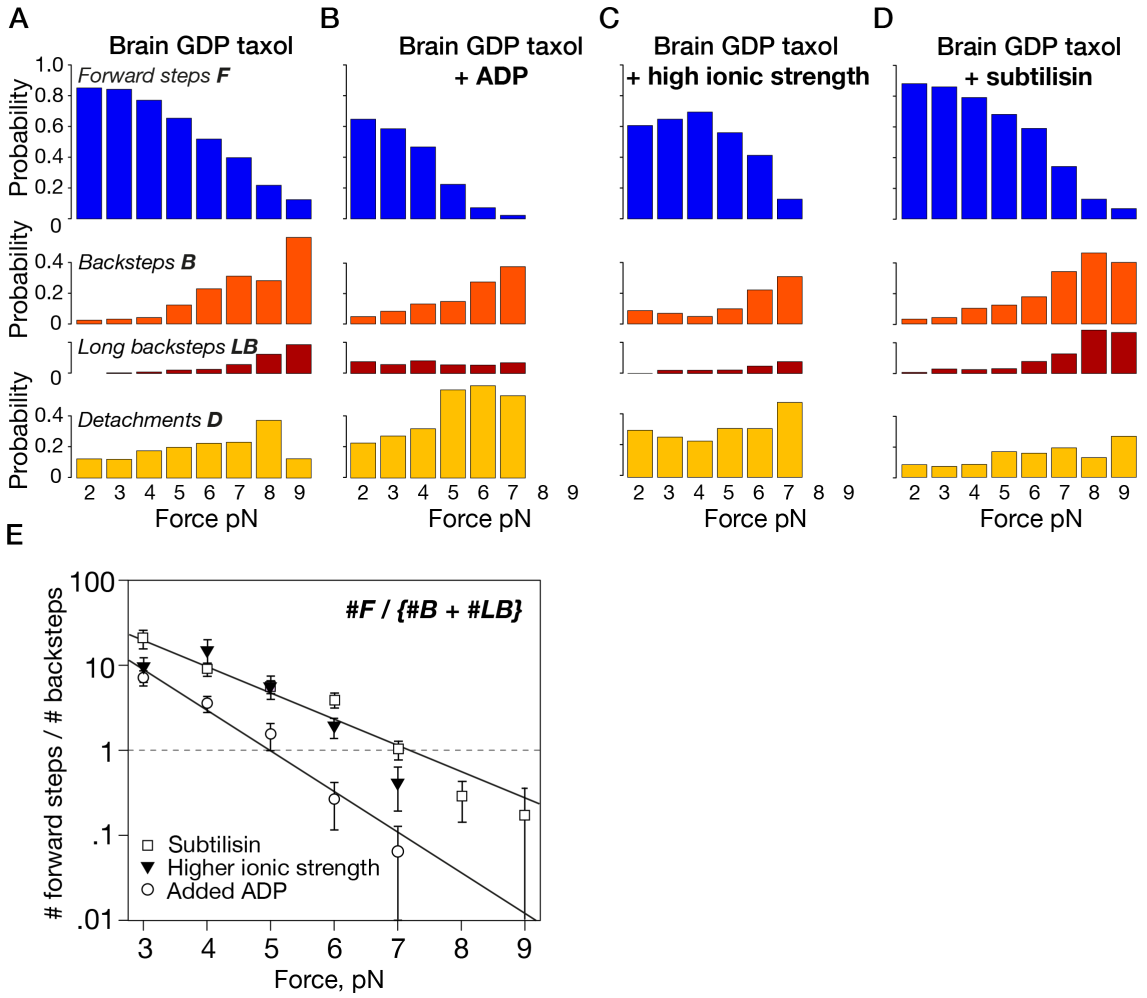

Fig. 4. Effects of changing conditions on step-event probabilities under load (*A*) Brain GDP taxol MTs. (*B*) Brain GDP taxol MTs with added 1mM ADP. (*C*) Brain GDP taxol MTs at higher ionic strength (BRB160 instead of BRB80) (*D*) Brain GDP taxol MTs treated with subtilisin (*E*) Effect of ADP, higher ionic strength and subtilisin treatment on #forward steps / #backsteps ratio, for kinesin stepping on GDP-taxol MTs under hindering load. ADP data fit parameters: k=-0.69, b=4.9. Subtilisin fit parameters k=-0.72, b=5.1 Higher ionic strength data did not obviously fit to a single-exponential. Errors are SE.

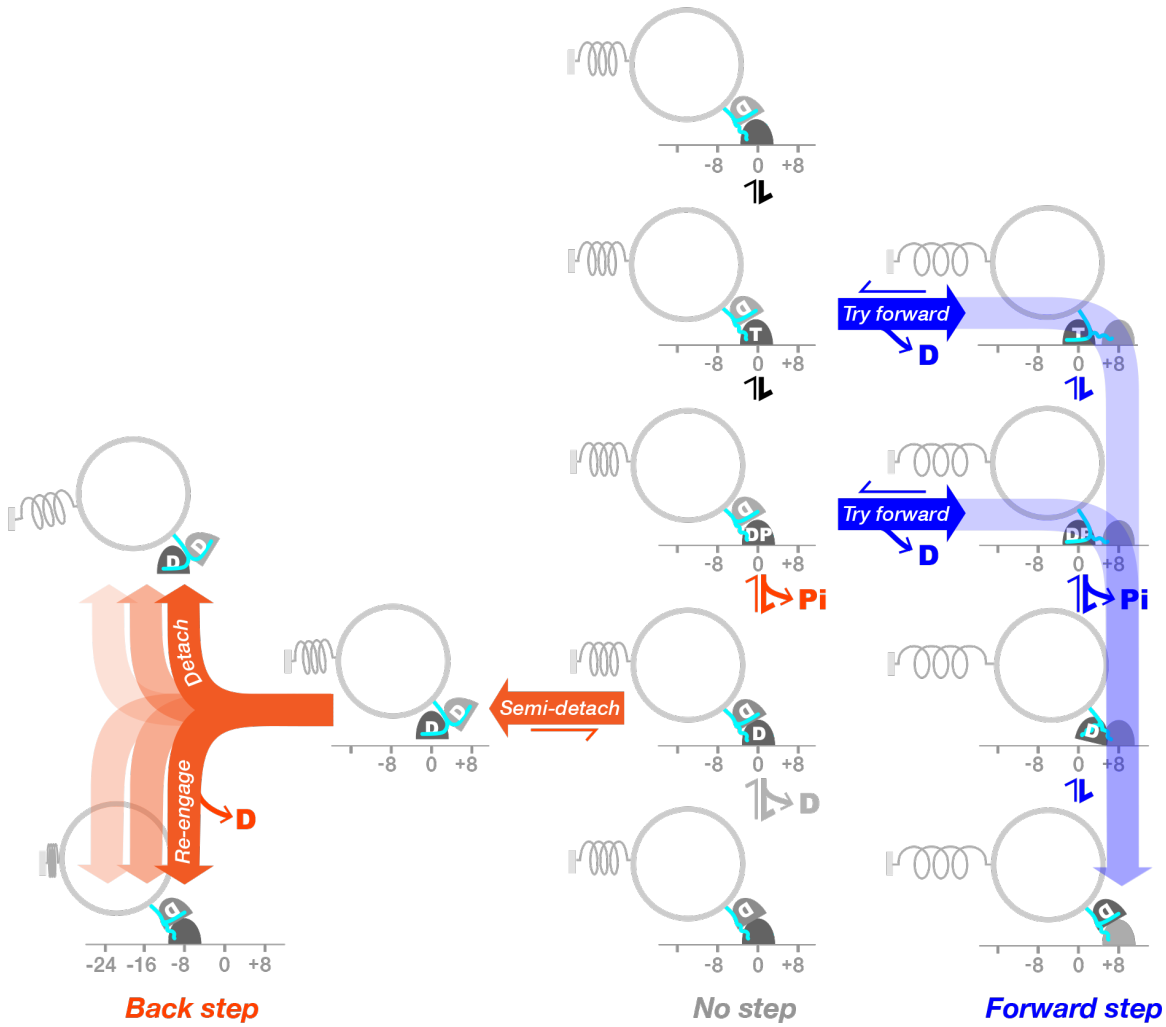

Fig. 5. Proposed model for backstepping via rescued detachment. During each cycle of ATP turnover, kinesin first attempts to step forward, within a time window opened by ATP binding and closed by Pi release (blue arrows). When forward stepping fails, kinesin adopts a weakly-bound K.ADP - K.ADP slip state. Backwards events and detachments (orange arrows) both originate from this semi-detached K.ADP-K.ADP state, which arises only following Pi release. For completeness, a presumptively minor futile process for ADP release whilst standing still (grey arrows) is also shown.